Structural Engineering and Mechanics, *Vol. 67, No. 1 (2018) 21-31*
DOI: https://doi.org/10.12989/sem.2018.67.1.021

Dynamic stability of nanocomposite Mindlin pipes conveying pulsating fluid flow subjected to magnetic field

Hemat Ali Esmaeili, Mehran Khaki* and Morteza Abbasi

Department of Mechanical Engineering, Sari Branch, Islamic Azad University, Sari, Iran

(Received February 20, 2018, Revised April 15, 2018, Accepted April 17, 2018)

Abstract. In this work, the dynamic stability of carbon nanotubes (CNTs) reinforced composite pipes conveying pulsating fluid flow is investigated. The pipe is surrounded by viscoelastic medium containing spring, shear and damper coefficients. Due to the existence of CNTs, the pipe is subjected to a 2D magnetic field. The radial induced force by pulsating fluid is obtained by the Navier-Stokes equation. The equivalent characteristics of the nanocomposite structure are calculated using Mori-Tanaka model. Based on first order shear deformation theory (FSDT) or Mindlin theory, energy method and Hamilton's principle, the motion equations are derived. Using harmonic differential quadrature method (HDQM) in conjunction with the Bolotin's method, the dynamic instability region (DIR) of the system is calculated. The effects of different parameters such as volume fraction of CNTs, magnetic field, boundary conditions, fluid velocity and geometrical parameters of pipe are shown on the DIR of the structure. Results show that with increasing volume fraction of CNTs, the DIR shifts to the higher frequency. In addition, the DIR of the structure will be happened at lower excitation frequencies with increasing the fluid velocity.

Keywords: dynamic stability; nanocomposite pipe; pulsating fluid; magnetic field; Bolotin method

1. Introduction

CNTs due to the excellent mechanical and thermal properties are a good candidate for the reinforce phase of composite structures. However, nanocomposite structures have been attracted more attention amongst researchers due to high mechanical and thermal properties and application in aerospace, automobile and etc. Since this paper studies the dynamic stability of nanocomposite pipes conveying pulsating fluid, the introduction divides into two parts including the theoretical works for the nanocomposite structures and structures conveying fluid.

Mechanical analysis of nanostructures has been reported by many researchers (Zemri 2015, Larbi Chaht 2015, Belkorissat 2015, Ahouel 2016, Bounouara 2016, Bouafia 2017, Besseghier 2017, Bellifa 2017, Mouffoki 2017, Khetir 2017). In the field of nanocomposite structures, Fiedler *et al.* (2006) highlighted the potential of the CNTs as nanofillers in polymers, but also stresses out the limitations and challenges one has to face dealing with nanoparticles in general. Esawi and Farag (2007) evaluated the technical and economic feasibility of using CNTs in reinforcing polymer composites. Natural frequencies characteristics of a continuously graded carbon nanotube-reinforced (CGCNTR) cylindrical panels based on the Eshelby-Mori-Tanaka approach was considered by Aragh *et al.* (2012). The influences of centrifugal and Coriolis forces on the free vibration behavior of rotating carbon nanotube reinforced composite (CNTRC) truncated conical shells were examined by Heydarpour *et al.* (2014). The effects of CNTs distributions on natural frequencies were studied by Hosseini (2013) for a functionally graded nanocomposite thick hollow cylinder reinforced by single-walled carbon nanotubes (SWCNTs) using a hybrid mesh-free method. Forced vibration behavior of nanocomposite beams reinforced by SWCNTs based on the Timoshenko beam theory along with von Kármán geometric nonlinearity was presented by Ansari *et al.* (2014). A linear buckling analysis was presented by Jam and Kiani (2015) for nanocomposite conical shells reinforced with SWCNTs subjected to lateral pressure. Analysis of free vibration of CNT reinforced functionally graded rotating cylindrical panels was presented by Lei *et al.* (2015) based on Extended rule of mixture for estimating the effective material properties of the resulting nanocomposite rotating panels. Garcıa-Macıas *et al.* (2016) provided results of static and dynamic numerical simulations of thin and moderately thick functionally graded (FG-CNTRC) skew plates with uniaxially aligned reinforcements. Moradi-Dastjerdi and Pourasghar (2016) reported on the effects of the aspect ratio and waviness index of CNTs on the free vibration and stress wave propagation of functionally graded (FG) nanocomposite cylinders that were reinforced by wavy SWCNT based on a mesh-free method.

None of the above mentioned works has been reported the structures conveying fluid. The dynamic stability of supported cylindrical pipes converying fluid, when the flow velocity is harmonically perturbed about a constant mean value, was considered by Ariaratnam and Namachchivaya (1986). A new method for the stability analysis of a pipe conveying fluid which pulsates periodically was presented by Jeong *et al.* (2007). Nonlinear dynamics of a hinged-hinged pipe conveying pulsatile fluid subjected to combination and principal parametric resonance in the

*Corresponding author
E-mail: mehran.khaki@gmail.com

ISSN: 1225-4568 (Print), 1598-6217 (Online)

presence of internal resonance was investigated by Panda and Kar (2008). Wang (2009) studied nonlinear dynamics of pipes conveying pulsating fluid using the Galerkin method and fourth order Runge-Kutta scheme. The natural frequency of fluid-structure interaction in pipeline conveying fluid was investigated by Huang *et al.* (2010) eliminated element-Galerkin method, and the natural frequency equations with different boundary conditions were obtained. Yu *et al.* (2011) studied the flexural vibration band gap in a periodic fluid-conveying pipe system based on the Timoshenko beam theory. For a single-walled CNT conveying fluid, the internal flow was considered by Liang and Su (2013) to be pulsating and viscous, and the resulting instability and parametric resonance of the CNT were investigated by the method of averaging. The vortex-induced vibrations of a long flexible pipe conveying pulsating flows were investigated by Dai *et al.* (2014) via a two-mode discretization of the governing differential equations. The stability and bifurcations of a hinged-hinged pipe conveying pulsating fluid with combination parametric and internal resonances were studied by Zhou *et al.* (2015) with both analytical and numerical methods. Attia (2016) presented dynamics of a straight supported pipe conveying a harmonically pulsating incompressible fluid flow. Raminnea *et al.* (2016) presented temperature-dependent nonlinear vibration and instability of embedded functionally graded (FG) pipes conveying viscous fluid-nanoparticle mixture. The free vibration analysis of fluid conveying Timoshenko pipeline with different boundary conditions using Differential Transform Method (DTM) and Adomian Decomposition Method (ADM) was investigated by Bozyigit *et al.* (2017). Vakili Tahami *et al.* (2017) studied Dynamic response of functionally graded Carbon nanotubes (FG-CNT) reinforced pipes conveying viscous fluid under accelerated moving load.

To the best of our knowledge, no investigation has been performed on the dynamic stability of nanocomposite pipes. The aim of this study is to present a mathematical model for dynamic stability analysis of pipes reinforced by CNTs conveying pulsating fluid. The nanocomposite pipe is surrounded by a viscoelastic medium which is simulated by visco-Pasternak foundation. The motion equations are derived using Hamilton's principle and FSDT. Applying HDQM and Bolotin's method, the DIR of structure is obtained. The influences of fluid velocity, geometrical parameters of pipe, viscoelastic foundation, percentage of CNTs in pipe and boundary conditions on the DIR of pipe are shown.

2. Structural definition

A schematic diagram of a pipe reinforced with CNTs conveying pulsating fluid embedded in a viscoelastic foundation is illustrate in Fig. 1 in which geometrical parameters of length L, average radius R and thickness h are also indicated. As shown in this figure, the viscoelastic foundation is simulated with spring, shear and damper elements.

There are many new theories for modeling of different

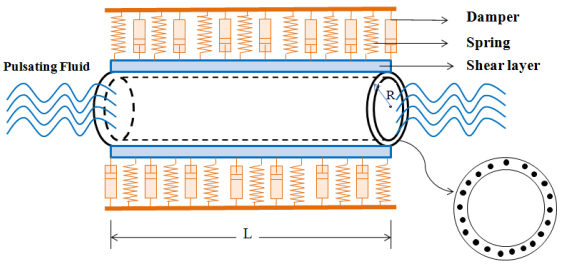

Fig. 1 Mathematical modeling of a nanocomposite pipe conveying pulsating fluid

structures. Some of the new theories have been used by Tounsi and co-authors (Bessaim 2013, Bouderba 2013, Belabed 2014, Ait Amar Meziane 2014, Zidi 2014, Hamidi 2015, Bourada 2015, Bousahla *et al.* 2016a, b, Beldjelili 2016, Boukhari 2016, Draiche 2016, Bellifa 2015, Attia 2015, Mahi 2015, Ait Yahia 2015, Bennoun 2016, El-Haina 2017, Menasria 2017, Chikh 2017). In order to calculate the middle-surface strain-displacement relations, the Mindlin theory is used. The displacement components of an arbitrary point based on this theory can be written as (Reddy 2002)

$$u_1(x,\theta,z,t) = u(x,\theta,t) + z\psi_x(x,\theta,t), \tag{1}$$

$$u_2(x,\theta,z,t) = v(x,\theta,t) + z\psi_\theta(x,\theta,t), \tag{2}$$

$$u_3(x,\theta,z,t) = w(x,\theta,t), \tag{3}$$

where $\psi_x(x,\theta,t)$ and $\psi_\theta(x,\theta,t)$ are the rotations of the normal to the mid-plane about x- and θ- directions, respectively. However, the nonlinear strain-displacement relations associated with the above displacement field can be derived as

$$\varepsilon_{xx} = \frac{\partial u}{\partial x} + \frac{1}{2}\left(\frac{\partial w}{\partial x}\right)^2 + z\frac{\partial \psi_x}{\partial x}, \tag{4}$$

$$\varepsilon_{\theta\theta} = \frac{\partial v}{R\partial\theta} + \frac{w}{R} + \frac{1}{2}\left(\frac{\partial w}{R\partial\theta}\right)^2 + z\frac{\partial \psi_\theta}{R\partial\theta}, \tag{5}$$

$$\gamma_{\theta z} = \frac{\partial w}{R\partial\theta} - \frac{v}{R} + \psi_\theta, \tag{6}$$

$$\gamma_{xz} = \frac{\partial w}{\partial x} + \psi_x, \tag{7}$$

$$\gamma_{x\theta} = \frac{\partial v}{\partial x} + \frac{\partial u}{R\partial\theta} + \frac{\partial w}{\partial x}\frac{\partial w}{R\partial\theta} + z\left(\frac{\partial \psi_x}{R\partial\theta} + \frac{\partial \psi_\theta}{\partial x}\right). \tag{8}$$

In this research the nanocomposite pipe is made of polymer reinforced by CNTs. However, the stress (σ_{ij})-strain (ε_{kl}) relation based on the Mori-Tanaka method as

(Mori and Tanaka 1973)

$$\begin{bmatrix}\sigma_{xx}\\ \sigma_{\theta\theta}\\ \tau_{\theta z}\\ \tau_{xz}\\ \tau_{x\theta}\end{bmatrix}=\begin{bmatrix}\underbrace{C_{11}}_{k+m} & \underbrace{C_{12}}_{l} & 0 & 0 & 0\\ \underbrace{C_{12}}_{l} & \underbrace{C_{22}}_{n} & 0 & 0 & 0\\ 0 & 0 & \underbrace{C_{44}}_{p} & 0 & 0\\ 0 & 0 & 0 & \underbrace{C_{55}}_{m} & 0\\ 0 & 0 & 0 & 0 & \underbrace{C_{66}}_{p}\end{bmatrix}\begin{Bmatrix}\varepsilon_{xx}\\ \varepsilon_{\theta\theta}\\ \gamma_{\theta z}\\ \gamma_{xz}\\ \gamma_{x\theta}\end{Bmatrix}, \tag{9}$$

where k, m, n, l and p are the stiffness coefficients which according to the Mori-Tanaka method can be given by

$$\begin{aligned}
k&=\frac{E_m\{E_m c_m+2k_r(1+\nu_m)[1+c_r(1-2\nu_m)]\}}{2(1+\nu_m)[E_m(1+c_r-2\nu_m)+2c_m k_r(1-\nu_m-2\nu_m^2)]}\\
l&=\frac{E_m\{c_m\nu_m[E_m+2k_r(1+\nu_m)]+2c_r l_r(1-\nu_m^2)]\}}{(1+\nu_m)[E_m(1+c_r-2\nu_m)+2c_m k_r(1-\nu_m-2\nu_m^2)]}\\
n&=\frac{E_m^2 c_m(1+c_r-c_m\nu_m)+2c_m c_r(k_r n_r-l_r^2)(1+\nu_m)^2(1-2\nu_m)}{(1+\nu_m)[E_m(1+c_r-2\nu_m)+2c_m k_r(1-\nu_m-2\nu_m^2)]}\\
&\quad+\frac{E_m[2c_m^2 k_r(1-\nu_m)+c_r n_r(1+c_r-2\nu_m)-4c_m l_r\nu_m]}{E_m(1+c_r-2\nu_m)+2c_m k_r(1-\nu_m-2\nu_m^2)}\\
p&=\frac{E_m[E_m c_m+2p_r(1+\nu_m)(1+c_r)]}{2(1+\nu_m)[E_m(1+c_r)+2c_m p_r(1+\nu_m)]}\\
m&=\frac{E_m[E_m c_m+2m_r(1+\nu_m)(3+c_r-4\nu_m)]}{2(1+\nu_m)\{E_m[c_m+4c_r(1-\nu_m)]+2c_m m_r(3-\nu_m-4\nu_m^2)\}}
\end{aligned} \tag{10}$$

where the subscripts m and r stand for matrix and reinforcement respectively; E_m and υ_m are the matrix Young's modulus and the Poisson's ratio; c_m and c_r are the volume fractions of the matrix and the CNTs, respectively; k_r, l_r, n_r, p_r, m_r are the Hills elastic modulus for the CNTs.

3. Motion equations

The total potential energy ($\prod$), of the embedded pipe is the sum of strain energy (U), kinetic energy (K) and the work done by the applied viscoelastic medium (W_V), pulsating fluid flow (W_F) and the force induced by magnetic field (W_M). The strain energy is

$$U=\frac{1}{2}\int\left(\sigma_{xx}\varepsilon_{xx}+\sigma_{\theta\theta}\varepsilon_{\theta\theta}+\tau_{x\theta}\gamma_{x\theta}+\tau_{xz}\gamma_{xz}+\tau_{\theta z}\gamma_{\theta z}\right)dV. \tag{11}$$

Combining of Eqs. (4)-(8) and (11) yields

$$\begin{aligned}
U=0.5\int\Bigg(&N_{xx}\left(\frac{\partial u}{\partial x}+\frac{1}{2}\left(\frac{\partial w}{\partial x}\right)^2\right)+N_{\theta\theta}\left(\frac{\partial v}{R\partial\theta}+\frac{w}{R}+\frac{1}{2}\left(\frac{\partial w}{R\partial\theta}\right)^2\right)\\
&+Q_\theta\left(\frac{\partial w}{R\partial\theta}-\frac{v}{R}+\psi_\theta\right)+Q_x\left(\frac{\partial w}{\partial x}+\psi_x\right)+N_{x\theta}\left(\frac{\partial v}{\partial x}+\frac{\partial u}{R\partial\theta}+\frac{\partial w}{\partial x}\frac{\partial w}{R\partial\theta}\right)\\
&+M_{xx}\frac{\partial\psi_x}{\partial x}+M_{\theta\theta}\frac{\partial\psi_\theta}{R\partial\theta}+M_{x\theta}\left(\frac{\partial\psi_x}{R\partial\theta}+\frac{\partial\psi_\theta}{\partial x}\right)\Bigg)dA,
\end{aligned} \tag{12}$$

where the resultant force and moments may be calculated as

$$\begin{bmatrix}N_{xx}\\ N_{\theta\theta}\\ N_{x\theta}\end{bmatrix}=\int_{-h/2}^{h/2}\begin{bmatrix}\sigma_{xx}\\ \sigma_{\theta\theta}\\ \tau_{x\theta}\end{bmatrix}dz, \tag{13}$$

$$\begin{bmatrix}M_{xx}\\ M_{\theta\theta}\\ M_{x\theta}\end{bmatrix}=\int_{-h/2}^{h/2}\begin{bmatrix}\sigma_{xx}\\ \sigma_{\theta\theta}\\ \sigma_{x\theta}\end{bmatrix}zdz, \tag{14}$$

$$\begin{bmatrix}Q_x\\ Q_\theta\end{bmatrix}=\int_{-h/2}^{h/2}\begin{bmatrix}k'\tau_{xz}\\ k'\tau_{z\theta}\end{bmatrix}dz, \tag{15}$$

where k' is shear correction factor.

The kinetic energy of the structure may be expressed as

$$K=\frac{\rho}{2}\int\left((\dot{u}_1)^2+(\dot{u}_2)^2+(\dot{u}_3)^2\right)dV, \tag{16}$$

where ρ is the density of nanocomposite pipe. By substituting Eqs. (1)-(3) in Eq. (16), we have

$$K=\frac{\rho}{2}\int\left(\left(\frac{\partial u}{\partial t}+z\frac{\partial\psi_x}{\partial t}\right)^2+\left(\frac{\partial v}{\partial t}+z\frac{\partial\psi_\theta}{\partial t}\right)^2+\left(\frac{\partial w}{\partial t}\right)^2\right)dV \tag{17}$$

By defining the following relations

$$\begin{Bmatrix}I_0\\ I_1\\ I_2\end{Bmatrix}=\int_{-h/2}^{h/2}\begin{bmatrix}\rho\\ \rho z\\ \rho z^2\end{bmatrix}dz, \tag{18}$$

Eq. (15) can be rewritten as below

$$\begin{aligned}
K=0.5\int\Bigg[&I_0\left(\left(\frac{\partial u}{\partial t}\right)^2+\left(\frac{\partial v}{\partial t}\right)^2+\left(\frac{\partial w}{\partial t}\right)^2\right)\\
&+2I_1\left(\frac{\partial u}{\partial t}\frac{\partial\psi_x}{\partial t}+\frac{\partial v}{\partial t}\frac{\partial\psi_\theta}{\partial t}\right)+I_2\left(\left(\frac{\partial\psi_x}{\partial t}\right)^2+\left(\frac{\partial\psi_\theta}{\partial t}\right)^2\right)\Bigg]dA.
\end{aligned} \tag{19}$$

The surrounded viscoelastic medium includes both normal and shear modulus with considering damping effect that modeled as follows (Ghavanloo 2010)

$$W_v=\int_A\left(-k_w w+k_g\nabla^2 w-c_v\left[\frac{\partial w}{\partial t}\right]\right)wdA, \tag{20}$$

where k_w, k_g and c_v are spring, shear and damping modulus, respectively.

In order to calculate the work down by fluid, the well-down Navies-Stokes equation is used as follows (Wang and Ni 2009)

$$\rho_f\frac{D\mathrm{V}}{Dt}=-\nabla\mathrm{P}+\mu\nabla^2\mathrm{V}+\mathrm{F}_{body\ force}, \tag{21}$$

where V=(v_r, v_θ, v_x) is the flow velocity in a cylindrical coordinate system, ρ_f, P and μ are fluid density, static pressure and fluid viscosity, respectively. In the Navies-Stokes equation, $\frac{D}{Dt}$ can be defined as follows considering axial fluid velocity

$$\frac{D}{Dt}=\frac{\partial}{\partial t}+v_x\frac{\partial}{\partial x}. \tag{22a}$$

At the point of contact between the inside tube and the internal fluid, their respective velocities and accelerations in the direction of flexural displacement become equal. These relationships thus can be written as

$$v_r = \frac{\partial w}{\partial t}. \tag{22b}$$

Using Eq. (22) and considering the axial fluid velocity, Eq. (21) can be expanded in z direction as follows

$$\begin{aligned}\frac{\partial p_r}{\partial r} = &-\rho_f\left(\frac{\partial^2 w}{\partial t^2}+2u_f\frac{\partial^2 w}{\partial x\,\partial t}+u_f^{\,2}\frac{\partial^2 w}{\partial x^2}\right)\\ &+\mu\left(\frac{\partial^3 w}{\partial x^2\partial t}+\frac{\partial^3 w}{R^2\partial\theta^2\partial t}+u_f\left(\frac{\partial^3 w}{\partial x^3}+\frac{\partial^3 w}{R^2\partial\theta^2\partial x}\right)\right).\end{aligned} \tag{23}$$

The work down by fluid can be calculated as follows

$$\begin{aligned}W_F &= \int (F_{fluid} = h_1\frac{\partial p_r}{\partial z})w\,dA\\ &= \int\left(-\rho_f h_1\left(\frac{\partial^2 w}{\partial t^2}+2u_f\frac{\partial^2 w}{\partial x\,\partial t}+u_f^{\,2}\frac{\partial^2 w}{\partial x^2}\right)\right.\\ &\left.+\mu h_1\left(\frac{\partial^3 w}{\partial x^2\partial t}+\frac{\partial^3 w}{R^2\partial\theta^2\partial t}+u_f\left[\frac{\partial^3 w}{\partial x^3}+\frac{\partial^3 w}{R^2\partial\theta^2\partial x}\right]\right)\right)w\,dA.\end{aligned} \tag{24}$$

The pulsating internal flow is assumed harmonically as follows

$$u_f = V_0(1+\beta\cos(\omega t)), \tag{25}$$

where V_0, β and ω are the mean flow velocity, the harmonic amplitude and pulsation frequency, respectively.

The Lorentz force due to a steady magnetic field, $\mathbf{H_0}$ can be obtained as follows (Kiani 2014)

$$\mathbf{f}_m = \eta\underbrace{\left(\nabla\times\underbrace{\left(\nabla\times\left(\mathbf{u}\times\mathbf{H}_0\right)\right)}_{\mathbf{h}}\right)}_{\mathbf{J}}\times\mathbf{H}_0, \tag{26}$$

where η, ∇, $\mathbf{u}$, $\mathbf{h}$ and $\mathbf{J}$ are the magnetic permeability of the SWCNTs, gradient operator, displacement field vector, disturbing vectors of magnetic field and current density, respectively. Noted that in this paper the magnetic field is assumed as $\mathbf{H_0} = H_x\delta_{x\vartheta}\hat{e}_x + H_\theta\delta_{\theta\vartheta}\hat{e}_\theta$ where δ is the Kronecker delta tensor. Using Eqs. (1)-(3), the Lorentz force per unit volume can be calculated as

$$f_x = \eta H_\theta^2\delta_{\theta\vartheta}\left[\left(\frac{\partial^2 u}{\partial x^2}+\frac{\partial^2 u}{R^2\partial\theta^2}\right)-z\left(\frac{\partial^3 w}{\partial x^3}+\frac{\partial^3 w}{R^2\partial x\partial\theta^2}\right)\right], \tag{27}$$

$$f_\theta = \eta H_x^2\delta_{x\vartheta}\left[\left(\frac{\partial^2 v}{\partial x^2}+\frac{\partial^2 v}{R^2\partial\theta^2}\right)-z\left(\frac{\partial^3 w}{R^3\partial\theta^3}+\frac{\partial^3 w}{R\partial\theta\partial x^2}\right)\right], \tag{28}$$

$$f_z = \eta\left[H_\theta^2\delta_{\theta\vartheta}\left(\frac{\partial^2 w}{R^2\partial\theta^2}-\frac{\partial^2 w}{\partial x^2}\right)+H_x^2\delta_{x\vartheta}\left(\frac{\partial^2 w}{\partial x^2}-\frac{\partial^2 w}{R^2\partial\theta^2}\right)\right]. \tag{29}$$

The generated forces and the bending moment caused by Lorentz force may be calculated by

$$\left(R_x^m, R_\theta^m, R_z^m\right) = \int_{-h/2}^{h/2}\left(f_x, f_\theta, f_z\right)dz, \tag{30}$$

$$\left(M_x^m, M_\theta^m, M_z^m\right) = \int_{-h/2}^{h/2}\left(f_x, f_\theta, f_z\right)z\,dz, \tag{31}$$

as a results

$$R_x^m = \eta h H_\theta^2\delta_{\theta\vartheta}\left(\frac{\partial^2 u}{\partial x^2}+\frac{\partial^2 u}{R^2\partial\theta^2}\right), \tag{32}$$

$$R_\theta^m = \eta h H_x^2\delta_{x\vartheta}\left(\frac{\partial^2 v}{\partial x^2}+\frac{\partial^2 v}{R^2\partial\theta^2}\right), \tag{33}$$

$$R_z^m = \eta h\left[H_\theta^2\delta_{\theta\vartheta}\left(\frac{\partial^2 w}{R^2\partial\theta^2}-\frac{\partial^2 w}{\partial x^2}\right)+H_x^2\delta_{x\vartheta}\left(\frac{\partial^2 w}{\partial x^2}-\frac{\partial^2 w}{R^2\partial\theta^2}\right)\right], \tag{34}$$

$$M_x^m = -\frac{\eta h^3 H_\theta^2}{12}\delta_{\theta\vartheta}\left(\frac{\partial^3 w}{\partial x^3}+\frac{\partial^3 w}{R^2\partial x\partial\theta^2}\right), \tag{35}$$

$$M_\theta^m = -\frac{\eta h^3 H_x^2}{12}\delta_{x\vartheta}\left(\frac{\partial^3 w}{R^3\partial\theta^3}+\frac{\partial^3 w}{R\partial\theta\partial x^2}\right). \tag{36}$$

Using Hamilton's principle, the variational form of the equations of motion can be expressed by

$$\delta\int_0^t\Pi\,dt = \delta\int_0^t\left[K-\left(U-\left\{W_V+W_F+W_M\right\}\right)\right]dt = 0. \tag{37}$$

By applying the Hamilton's principle and sorting of mechanical displacement, five governing equations are obtained as follows

$$\delta u: \quad \frac{\partial N_{xx}}{\partial x}+\frac{\partial N_{x\theta}}{R\partial\theta}+R_x^m = I_0\frac{\partial^2 u}{\partial t^2}+I_1\frac{\partial^2\psi_x}{\partial t^2}, \tag{38}$$

$$\delta v: \quad \frac{\partial N_{x\theta}}{\partial x}+\frac{\partial N_{\theta\theta}}{R\partial\theta}+\frac{Q_\theta}{R}+R_\theta^m = I_0\frac{\partial^2 v}{\partial t^2}+I_1\frac{\partial^2\psi_\theta}{\partial t^2}, \tag{39}$$

$$\begin{aligned}\delta w: \quad &\frac{\partial Q_x}{\partial x}+\frac{\partial Q_\theta}{R\partial\theta}-k_w w+k_g\nabla^2 w-c_v\dot{w}\\ &-\rho_f h_1\left(\frac{\partial^2 w}{\partial t^2}+2u_f\frac{\partial^2 w}{\partial x\,\partial t}+u_f^{\,2}\frac{\partial^2 w}{\partial x^2}\right)+R_z^m\\ &+\mu h_1\left(\frac{\partial^3 w}{\partial x^2\partial t}+\frac{\partial^3 w}{R^2\partial\theta^2\partial t}+u_f\right.\\ &\left.\left(\frac{\partial^3 w}{\partial x^3}+\frac{\partial^3 w}{R^2\partial\theta^2\partial x}\right)\right) = I_0\frac{\partial^2 w}{\partial t^2},\end{aligned} \tag{40}$$

$$\delta\psi_x: \quad \frac{\partial M_{xx}}{\partial x}+\frac{\partial M_{x\theta}}{R\partial\theta}-Q_x+M_x^m = I_1\frac{\partial^2 u}{\partial t^2}+I_2\frac{\partial^2\psi_x}{\partial t^2}, \tag{41}$$

$$\delta\psi_\theta: \quad \frac{\partial M_{x\theta}}{\partial x}+\frac{\partial M_{\theta\theta}}{R\partial\theta}-Q_\theta+M_\theta^m = I_1\frac{\partial^2 v}{\partial t^2}+I_2\frac{\partial^2\psi_\theta}{\partial t^2}, \tag{42}$$

Using Eqs. (4)-(9), the resultant force and moments can be written as

$$N_{xx}=A_{11}\left(\frac{\partial u}{\partial x}+\frac{1}{2}\left(\frac{\partial w}{\partial x}\right)^2\right)+B_{11}\left(\frac{\partial \psi_x}{\partial x}\right)$$
$$+A_{12}\left(\frac{\partial v}{R\partial\theta}+\frac{w}{R}+\frac{1}{2}\left(\frac{\partial w}{R\partial\theta}\right)^2\right)+B_{12}\left(\frac{\partial \psi_\theta}{R\partial\theta}\right), \tag{43}$$

$$N_{\theta\theta}=A_{12}\left(\frac{\partial u}{\partial x}+\frac{1}{2}\left(\frac{\partial w}{\partial x}\right)^2\right)+B_{12}\left(\frac{\partial \psi_x}{\partial x}\right)$$
$$+A_{22}\left(\frac{\partial v}{R\partial\theta}+\frac{w}{R}+\frac{1}{2}\left(\frac{\partial w}{R\partial\theta}\right)^2\right)+B_{22}\left(\frac{\partial \psi_\theta}{R\partial\theta}\right), \tag{44}$$

$$N_{x\theta}=A_{66}\left(\frac{\partial u}{R\partial\theta}+\frac{\partial v}{\partial x}+\frac{\partial w}{\partial x}\frac{\partial w}{R\partial\theta}\right)$$
$$+B_{66}\left(\frac{\partial \psi_x}{R\partial\theta}+\frac{\partial \psi_\theta}{\partial x}\right), \tag{45}$$

$$Q_x=A_{55}\left(\frac{\partial w}{\partial x}+\psi_x\right), \tag{46}$$

$$Q_\theta=A_{44}\left(\frac{\partial w}{R\partial\theta}-\frac{v}{R}+\psi_\theta\right), \tag{47}$$

$$M_{xx}=B_{11}\left(\frac{\partial u}{\partial x}+\frac{1}{2}\left(\frac{\partial w}{\partial x}\right)^2\right)+D_{11}\left(\frac{\partial \psi_x}{\partial x}\right)$$
$$+B_{12}\left(\frac{\partial v}{R\partial\theta}+\frac{w}{R}+\frac{1}{2}\left(\frac{\partial w}{R\partial\theta}\right)^2\right)+D_{12}\left(\frac{\partial \psi_\theta}{R\partial\theta}\right), \tag{48}$$

$$M_{\theta\theta}=B_{12}\left(\frac{\partial u}{\partial x}+\frac{1}{2}\left(\frac{\partial w}{\partial x}\right)^2\right)+D_{12}\left(\frac{\partial \psi_x}{\partial x}\right)$$
$$+B_{22}\left(\frac{\partial v}{R\partial\theta}+\frac{w}{R}+\frac{1}{2}\left(\frac{\partial w}{R\partial\theta}\right)^2\right)+D_{22}\left(\frac{\partial \psi_\theta}{R\partial\theta}\right), \tag{49}$$

where

$$\left(A_{11},A_{12},A_{22},A_{44},A_{55},A_{66}\right)=$$
$$\int_{-h/2}^{h/2}\left(C_{11},C_{12},C_{22},C_{44},C_{55},C_{66}\right)dz, \tag{50}$$

$$\left(B_{11},B_{12},B_{22},B_{66}\right)=$$
$$\int_{-h/2}^{h/2}\left(C_{11},C_{12},C_{22},C_{66}\right)z\,dz, \tag{51}$$

$$\left(D_{11},D_{12},D_{22},D_{66}\right)=$$
$$\int_{-h/2}^{h/2}\left(C_{11},C_{12},C_{22},C_{66}\right)z^2dz, \tag{52}$$

Substituting Eqs. (43)-(49) into Eqs. (38)-(42) yields

$$A_{11}\left(\frac{\partial^2 u}{\partial x^2}+\frac{\partial w}{\partial x}\frac{\partial^2 w}{\partial x^2}\right)+B_{11}\left(\frac{\partial^2 \psi_x}{\partial x^2}\right)$$
$$+A_{12}\left(\frac{\partial^2 v}{R\partial x\,\partial\theta}+\frac{\partial w}{R\partial x}+\frac{\partial w}{R\partial\theta}\frac{\partial^2 w}{R\partial x\,\partial\theta}\right)$$
$$+B_{12}\left(\frac{\partial^2 \psi_\theta}{R^2\partial x\,\partial\theta}\right)+\frac{B_{66}}{R}\left(\frac{\partial^2 \psi_x}{R\partial\theta^2}+\frac{\partial^2 \psi_\theta}{\partial x\,\partial\theta}\right)$$
$$+\frac{A_{66}}{R}\left(\frac{\partial^2 u}{R\partial\theta^2}+\frac{\partial^2 v}{\partial x\,\partial\theta}+\frac{\partial^2 w}{\partial x\,\partial\theta}\frac{\partial w}{R\partial\theta}+\frac{\partial w}{\partial x}\frac{\partial^2 w}{R\partial\theta^2}\right)$$
$$+\eta h H_\theta^2\delta_{\theta 9}\left(\frac{\partial^2 u}{\partial x^2}+\frac{\partial^2 u}{R^2\partial\theta^2}\right)=I_0\frac{\partial^2 u}{\partial t^2}+I_1\frac{\partial^2 \psi_x}{\partial t^2} \tag{53}$$

$$A_{66}\left(\frac{\partial^2 u}{R\partial\theta\partial x}+\frac{\partial^2 v}{\partial x^2}+\frac{\partial^2 w}{\partial x^2}\frac{\partial w}{R\partial\theta}+\frac{\partial w}{\partial x}\frac{\partial^2 w}{R\partial\theta\partial x}\right)$$
$$+B_{66}\left(\frac{\partial^2 \psi_x}{R\partial\theta\partial x}+\frac{\partial^2 \psi_\theta}{\partial x^2}\right)+\frac{A_{12}}{R}\left(\frac{\partial^2 u}{\partial x\,\partial\theta}+\frac{\partial w}{\partial x}\frac{\partial^2 w}{\partial x\,\partial\theta}\right)$$
$$+\frac{B_{12}}{R}\left(\frac{\partial^2 \psi_x}{\partial x\,\partial\theta}\right)+\frac{A_{22}}{R}\left(\frac{\partial^2 v}{R\partial\theta^2}+\frac{\partial w}{R\partial\theta}+\frac{\partial w}{R\partial\theta}\frac{\partial^2 w}{R\partial\theta^2}\right)$$
$$+\frac{B_{22}}{R}\left(\frac{\partial^2 \psi_\theta}{R^2\partial\theta^2}\right)+\eta h H_x^2\delta_{x9}\left(\frac{\partial^2 v}{\partial x^2}+\frac{\partial^2 v}{R^2\partial\theta^2}\right)=I_0\frac{\partial^2 v}{\partial t^2} \tag{54}$$

$$A_{55}\left(\frac{\partial^2 w}{\partial x^2}+\frac{\partial \psi_x}{\partial x}\right)+\frac{A_{44}}{R}\left(\frac{\partial^2 w}{R\partial\theta^2}-\frac{\partial v}{R\partial\theta}+\frac{\partial \psi_\theta}{\partial\theta}\right)$$
$$-k_W w+k_g\nabla^2 w-c_v\dot{w}$$
$$-\rho_f h_1\left(\frac{\partial^2 w}{\partial t^2}+2u_f\frac{\partial^2 w}{\partial x\,\partial t}+u_f{}^2\frac{\partial^2 w}{\partial x^2}\right)$$
$$+\mu h_1\left(\frac{\partial^3 w}{\partial x^2\partial t}+\frac{\partial^3 w}{R^2\partial\theta^2\partial t}+u_f\left(\frac{\partial^3 w}{\partial x^3}+\frac{\partial^3 w}{R^2\partial\theta^2\partial x}\right)\right)=I_0\frac{\partial^2 w}{\partial t^2}, \tag{55}$$

$$B_{11}\left(\frac{\partial^2 u}{\partial x^2}+\frac{\partial w}{\partial x}\frac{\partial^2 w}{\partial x^2}\right)+D_{11}\left(\frac{\partial^2 \psi_x}{\partial x^2}\right)$$
$$+B_{12}\left(\frac{\partial^2 v}{R\partial\theta\partial x}+\frac{\partial w}{\partial x}+\frac{\partial^2 w}{R\partial\theta\partial x}\right)+D_{12}\left(\frac{\partial^2 \psi_\theta}{R\partial\theta\partial x}\right)$$
$$+\frac{B_{66}}{R}\left(\frac{\partial^3 u}{R\partial x\,\partial\theta^2}+\frac{\partial^2 v}{\partial x\,\partial\theta}+\frac{\partial^2 w}{\partial x\,\partial\theta}\frac{\partial w}{R\partial\theta}+\frac{\partial w}{\partial x}\frac{\partial^2 w}{R\partial\theta^2}\right)$$
$$+\frac{D_{66}}{R}\left(\frac{\partial^2 \psi_x}{R\partial\theta^2}+\frac{\partial^2 \psi_\theta}{\partial x\,\partial\theta}\right)-A_{55}\left(\frac{\partial w}{\partial x}+\psi_x\right)$$
$$+\frac{\eta h^3 H_\theta^2}{12}\delta_{\theta 9}\left(\frac{\partial^2 \psi_x}{\partial x^2}+\frac{\partial^2 \psi_x}{R^2\partial\theta^2}\right)=I_1\frac{\partial^2 u}{\partial t^2}+I_2\frac{\partial^2 \psi_x}{\partial t^2} \tag{56}$$

In this paper, three types of boundary conditions are considered as

• Simple-Simple (SS)

$$x=0,L\Rightarrow u=v=w=\phi_\theta=M_x=0, \tag{58}$$

• Clamped- Clamped (CC)

$$x=0,L\Rightarrow u=v=w=\phi_x=\phi_\theta=0, \tag{59}$$

• Clamped- Simple (CS)

$$\begin{aligned} &x=0\Rightarrow u=v=w=\phi_x=\phi_\theta=0,\\ &x=L\Rightarrow u=v=w=\phi_x=M_x=0. \end{aligned} \tag{60}$$

4. Solution procedures

HDQM is used in this study to solve the motion equations. In this method, the differential equations change into first algebraic equations with first order and weighting coefficients. In other words, the partial derivatives of a function (F) are approximated by a specific variable, at discontinuous points in domain as a set of weighting series and its amount represent by the function itself at that point and other points throughout the domain. Let F be a function of x and θ in the domain of ($0<x<L$, $0<\theta<2\pi$). Based on this method, the derivates with respect to x and θ can be written as (Civalek 2004)

$$\frac{d^n F(x_i,\theta_j)}{dx^n}=\sum_{k=1}^{N_x} A_{ik}^{(n)} F(x_k,\theta_j) \qquad n=1,...,N_x-1, \tag{61a}$$

$$\frac{d^m F(x_i,\theta_j)}{d\theta^m}=\sum_{l=1}^{N_\theta} B_{jl}^{(m)} F(x_i,\theta_l) \qquad m=1,...,N_\theta-1, \tag{61b}$$

$$\frac{d^{n+m} F(x_i,\theta_j)}{dx^n d\theta^m}=\sum_{k=1}^{N_x}\sum_{l=1}^{N_\theta} A_{ik}^{(n)} B_{jl}^{(m)} F(x_k,\theta_l), \tag{61c}$$

where $A_{ik}^{(n)}$ and $B_{jl}^{(m)}$ are the weighting coefficients associated with n^{th}-order partial derivative of F(x,θ) with respect to x at the discrete point x_i and m^{th}-order derivative with respect to θ at θ_i, respectively, whose recursive formulae can be written as

$$A_{ij}^{(1)}=\begin{cases} \dfrac{(\pi/2)M(x_i)}{M(x_j)\sin[(x_i-x_j)/2]\pi} & for \quad i\neq j, \quad i,j=1,2,...,N_x,\\ -\sum\limits_{\substack{j=1\\ i\neq j}}^{N_x} A_{ij}^{(1)} & for \quad i=j, \quad i,j=1,2,...,N_x \end{cases} \tag{62a}$$

$$B_{ij}^{(1)}=\begin{cases} \dfrac{(\pi/2)P(\theta_i)}{P(\theta_j)\sin[(\theta_i-\theta_j)]\pi} & for \quad i\neq j, \quad i,j=1,2,...,N_\theta,\\ -\sum\limits_{\substack{j=1\\ i\neq j}}^{N_\theta} B_{ij}^{(1)} & for \quad i=j, \quad i,j=1,2,...,N_\theta \end{cases} \tag{62b}$$

where

$$M(x_i)=\prod_{\substack{j=1\\ j\neq i}}^{N_x}\sin\left(\frac{(x_i-x_j)\pi}{2}\right) \tag{63}$$

$$P(\theta_i)=\prod_{\substack{j=1\\ j\neq i}}^{N_\theta}\sin\left(\frac{(\theta_i-\theta_j)\pi}{2}\right) \tag{64}$$

In addition, for higher order derivatives we have

$$A_{ij}^{(n)}=n\left(A_{ii}^{(n-1)}A_{ij}^{(1)}-\pi ctg\left(\frac{x_i-x_j}{2}\right)\pi\right) \tag{65}$$

$$B_{ij}^{(m)}=m\left(B_{ii}^{(m-1)}B_{ij}^{(1)}-\pi ctg\left(\frac{\theta_i-\theta_j}{2}\right)\pi\right) \tag{66}$$

A more superior choice for the positions of the grid points is Chebyshev polynomials as expressed in [26]

$$x_i=\frac{L}{2}\left[1-\cos\left(\frac{i-1}{N_x-1}\right)\pi\right] \tag{67}$$

$$\theta_i=\frac{2\pi}{2}\left[1-\cos\left(\frac{i-1}{N_\theta-1}\right)\pi\right] \tag{68}$$

Applying HDQM and using Eqs. (58)-(60) to motion equations and boundary conditions results governing equations as set of algebraic.

$$\begin{aligned} &\left([K]+u_f[K]^f+u_f{}^2[K]^{ff}\right)\begin{Bmatrix} d_b\\ d_d\end{Bmatrix}\\ &+\left([C]+u_f[C]^f\right)\begin{Bmatrix}\dot{d}_b\\ \dot{d}_d\end{Bmatrix}+[M]\begin{Bmatrix}\ddot{d}_b\\ \ddot{d}_d\end{Bmatrix}=0. \end{aligned} \tag{69}$$

where $[K]$ and $[C]$ are stiffness matrix and damping, respectively and $[M]$ is matrices of mass; d_b and d_d are related to the boundary and domain points, respectively. Finally, by substituting Eq. (25) to Eq. (69), we have

$$\begin{aligned} &\left([K]+\left(u_f\left[1+\alpha\cos(\omega t)\right]\right)[K]^f+\left(u_f\left[1+\alpha\cos(\omega t)\right]\right)^2[K]^{ff}\right)\{d\}\\ &+\left([C]+\left(u_f\left[1+\alpha\cos(\omega t)\right]\right)[C]^f\right)\{\dot{d}\}\\ &+[M]\{\ddot{d}\}=0, \end{aligned} \tag{70}$$

In the above equations $[K]^f$, $[K]^{ff}$ and $[C]^f$ are stiffness matrix coefficients, damping coefficient matrix coefficients of pulsating fluid. To solve the Eq. (70), the Bolotin's method is used. In this way displacement vector $\{d\}$ be considered as follows (Patel 2006)

$$\{d\}=\sum_{k=1,3,...}^{\infty}\left[\{a\}_k\sin\frac{k\omega t}{2}+\{b\}_k\cos\frac{k\omega t}{2}\right], \tag{71}$$

According to studies, the first dynamic range of the most important and largest range of shows. Finally, by substituting the Eq. (71) in Eq. (70) and separate *sinus* and *cosinus* coefficients, we have

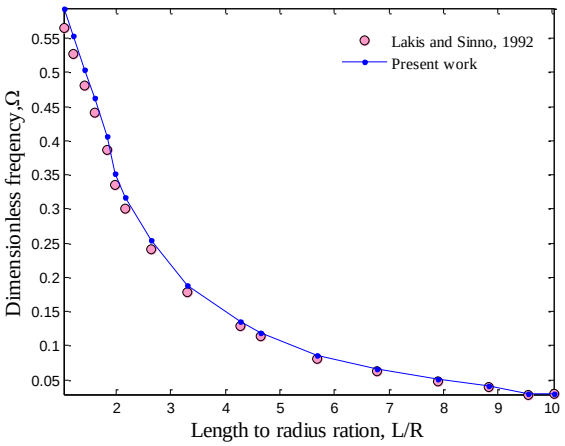

Fig. 2 Dimensionless frequency of a pipe versus length to radius ratio for the first mode

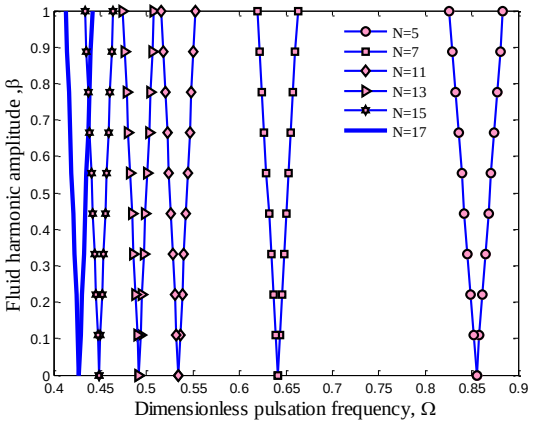

Fig. 3 Convergence and accuracy of HDQM

$$\left|\left([K]+\left(1\pm\frac{\alpha}{2}\right)[K]^{f}+\left(1\pm\alpha+\frac{\alpha^{2}}{2}\right)[K]^{ff}\right)+\left(\pm[C]\frac{\omega^{2}}{2}+\left(\frac{\alpha\omega}{4}\pm\frac{\omega}{2}\right)[C]^{f}\right)-[M]\frac{\omega^{2}}{4}\right|=0. \quad (72)$$

Eq. (38) is an eigenvalue problem which based on a direct iterative method, the variation of ω with respect to α as DIR of system can be obtained.

5. Numerical results and discussion

In this research, dynamic stability of nanocomposite pipes conveying pulsation fluid flow is studied. The pipe is made from polyethylene (PE) with the Yong modulus of E_m=0.3 *Gpa*, Poisson's ration of v_m=0.3, length to thickness ratio of L/h=40 and thickness to radius ratio of h/R=0.02, which is reinforced with CNTs with the Hills elastic modulus reported in [22]. the fluid inside the pipe is water with the density of ρ_f=1000 Kg/m^3 and viscosity of μ=8.9×10^{-4} *Pa.s*.

At the first, the validation of presented results is investigated. For this purpose, neglecting CNTs (c_r=0), viscoelastic medium and fluid, dimensionless frequency ($\Omega=\omega R[\rho_m(1-\upsilon_m{}^2)]^{0.5}$) of a pipe h/R=0.02 is plotted in Fig. 2 against length to radius ratio for the first mode. It can be seen that presented results are in a good agreement with Ref. (Lakis and Sinno 1992).

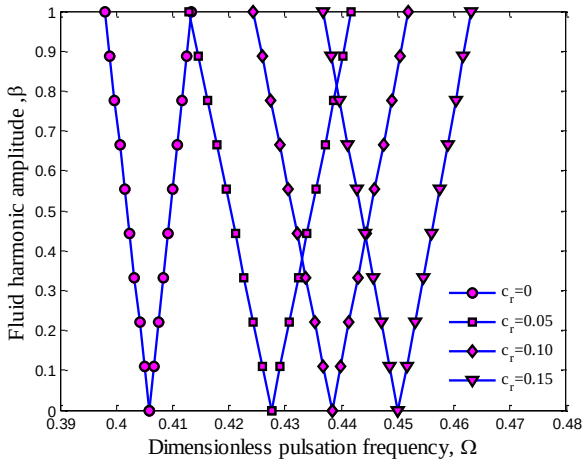

Fig. 4 The effects of CNTs volume percent on the DIR of structure

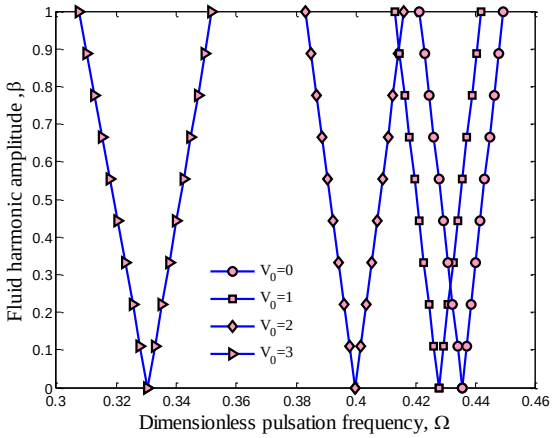

Fig. 5 The effects of dimensionless flow velocity on the DIR of structure

The convergence and accuracy of HDQM is studied in Fig. 3. As shown, the fluid harmonic amplitude is plotted versus dimensionless pulsation frequency for different grid point numbers. It can be concluded that with increasing the grid point numbers, the dimensionless pulsation frequency decreases until in N=17, the results become converge. However, the result of this work are reported for N=17.

The effects of different parameter on the DIR of structure are discussed. In all of the figures, the fluid harmonic amplitude is plotted versus dimensionless pulsation frequency. In these figures, the regions inside and outside the boundary curves are correspond to unstable (parametric resonance) and stable regions, respectively.

Fig. 4 shows the effects of CNTs volume percent on the DIR of nanocomposite pipe. It is observed that with the increase of the CNT volume percent, the dimensionless pulsation frequency increases and the DIR of structure shifts to right. Since the elastic stiffness and density of

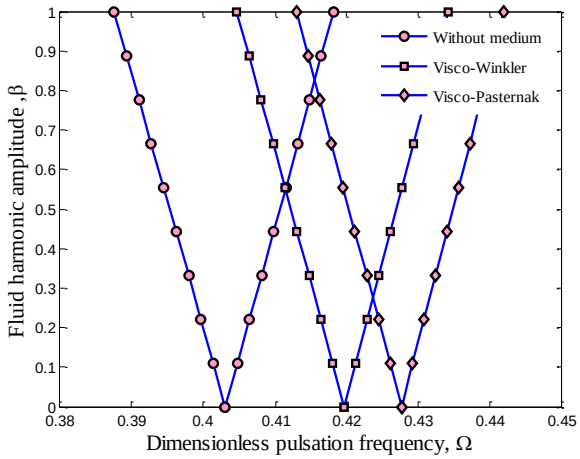

Fig. 6 The effects of surrounding viscoelastic foundation on the DIR of structure

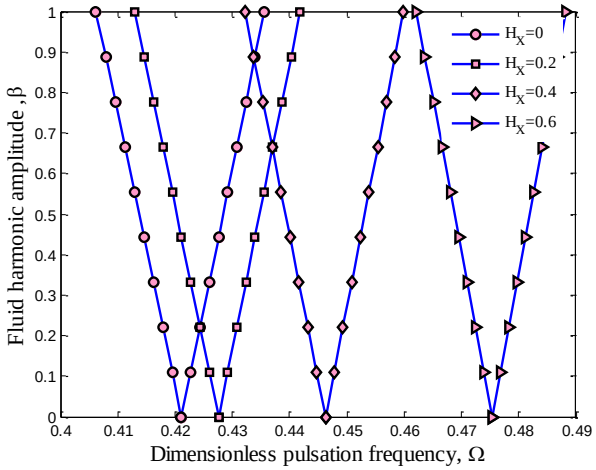

Fig. 7 The effects of longitudinal magnetic field intensity on the DIR of structure

CNTs are higher than PE, with increasing volume percent of CNTs in polymer, the equivalent stiffness coefficients as well as the density increase, and this makes the system stronger, and the instability occurs later.

Fig. 5 presents the effect of dimensionless flow velocity (V_0=$v_0[\rho_m/E_m]^{0.5}$) on the DIR of system. As can be seen, with increasing fluid velocity, the DIR occurs in lower pulsation frequencies. In addition, the greater fluid velocity leads to large instability zone and low pulsation frequency.

In order to show the effects of surrounding viscoelastic foundation, Fig. 6 depicts DIR of structure. Three different viscoelastic medium are considered namely as without viscoelastic medium, visco-Winkler medium and visco-Pasternak mediums. As can be seen considering viscoelastic foundation increases the magnitude of dimensionless pulsation frequency and subsequently, DIR shifts to right. It is due to the fact that putting the system in a viscoelastic medium makes the system more stable and stiffer. It is also concluded that the DIR of visco-Pasternak model is higher than visco-Winkler. It is because nonlinear visco-Pasternak model considers not only the normal stresses but also the transverse shear deformation and continuity among the spring elements.

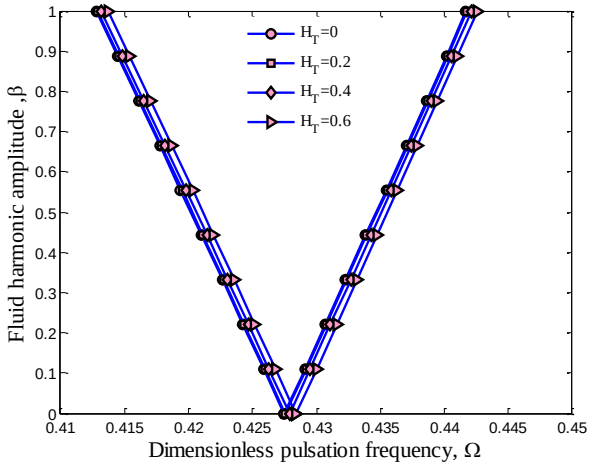

Fig. 8 The effects of circumferential magnetic field intensity on the DIR of structure

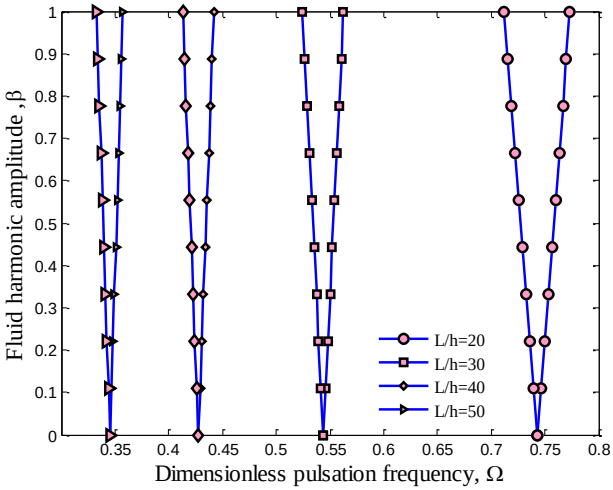

Fig. 9 The effects of length to the thickness ratio on the DIR of structure

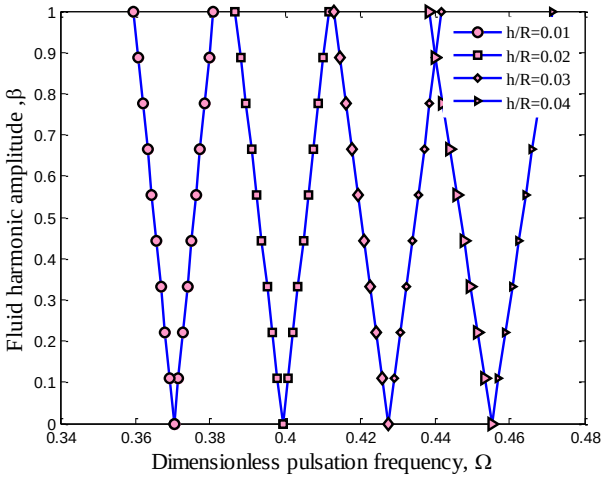

Fig. 10 The effects of thickness to radius ratio on the DIR of structure

Figs. 7 and 8 show, respectively, longitudinal and circumferential magnetic field intensity on the variations of the dimensionless pulsation frequency versus the fluid

pulsation amplitude. It can be observed that increment of longitudinal and circumferential magnetic field intensity makes the system more stable, hence the DIR and dimensionless pulsation frequency shift to right and increase. Comparing the effect of longitudinal and circumferential magnetic field intensity, it can be concluded that the effect of longitudinal magnetic field intensity on the DIR of structure is higher than circumferential one.

Variation of length to the thickness ratio and thickness to radius ratio on the DIR of structure are observed in Figs. 9 and 10. Ii is clear that the increase in length to the thickness ratio decreases the pulsation frequency while increasing thickness to radius ratio increases the pulsation frequency. It is due to the fact that with increasing length to the thickness ratio and thickness to radius ratio, the stiffness of structure decrease and increases, respectively.

6. Conclusions

Dynamic stability of CNT reinforced pipes conveying pulsating fluid flow was presented in this article. The external surface of pipe was surrounded by viscoelastic foundation. The radial applied force by the fluid was derived using Navier-Stokes equation. Based on Mindlin theory, energy method and Hamilton's principal, the motion equations were derived. Applying HDQM and Bolotin method, the DIR of structure was obtained. The obtained results by were listed as follows:

• Increasing the volume percent of CNTs in polymer matrix leads to increase in pulsation frequency, so the system becomes more stable.

• Increasing the fluid velocity, pulsation frequency decreases and the pipe becomes susceptible to instability.

• Increasing the magnetic field leads to increase the pulsation frequency and the stability of system.

• The high values of length to thickness ratio, reduces the pulsation frequency and closes the system to the unstable state.

• Considering viscoelastic foundation leads to higher pulsation frequency.

References

Ahouel, M., Houari, M.S.A., Adda Bedia, E.A. and Tounsi, A. (2016), "Size-dependent mechanical behavior of functionally graded trigonometric shear deformable nanobeams including neutral surface position concept", *Steel Compos. Struct.*, **20**(5), 963-981.

Ansari, R., Faghih Shojaei, M. and Mohammadi, V. (2014), "Nonlinear forced vibration analysis of functionally graded carbon nanotube-reinforced composite Timoshenko beams", *Compos. Struct.*, **113**, 316-327.

Aragh, S.B., Nasrollah Barati, A.H. and Hedayati, H. (2012), "Eshelby-Mori-Tanaka approach for vibrational behavior of continuously graded carbon nanotube-reinforced cylindrical panels", *Compos. Part B: Eng.*, **43**(4), 1943-1954.

Ariaratnam, S.T. and Namachchivay, N.S. (1986), "Dynamic stability of pipes conveying pulsating fluid", *J. Sound Vibr.*, **107**(2), 215-230.

Attia, A., Tounsi, A., Adda Bedia, E.A. and Mahmoud, S.R. (2015), "Free vibration analysis of functionally graded plates with temperature-dependent properties using various four variable refined plate theories", *Steel Compos. Struct.*, **18**(1), 187-212.

Attia, E.M. (2016), "Vibrations analysis of ruptured pipe conveying pulsating fluid flow and supported by a magnetorheological damper", *J. Vibroeng.*, **18**(5), 3242-3257.

Belabed, Z., Houari, M.S.A., Tounsi, A., Mahmoud, S.R. and Bég, O.A. (2014), "An efficient and simple higher order shear and normal deformation theory for functionally graded material (FGM) plates", *Compos.: Part B*, **60**, 274-283.

Beldjelili, Y., Tounsi, A. and Mahmoud, S.R. (2016), "Hygro-thermo-mechanical bending of S-FGM plates resting on variable elastic foundations using a four-variable trigonometric plate theory", *Smart Struct. Syst.*, **18**(4), 755-786.

Belkorissat, I., Houari, M.S.A., Tounsi, A. and Hassan, S. (2015), "On vibration properties of functionally graded nano-plate using a new nonlocal refined four variable model", *Steel Compos. Struct.*, **18**(4), 1063-1081.

Bellifa, H., Benrahou, K.H., Bousahla, A.A., Tounsi, A. and Mahmoud, S.R. (2017), "A nonlocal zeroth-order shear deformation theory for nonlinear postbuckling of nanobeams", *Struct. Eng. Mech.*, **62**(6), 695-702.

Bellifa, H., Benrahou, K.H., Hadji, L., Houari, M.S.A. and Tounsi, A. (2016), "Bending and free vibration analysis of functionally graded plates using a simple shear deformation theory and the concept the neutral surface position", *J. Braz. Soc. Mech. Sci. Eng.*, **38**(1), 265-275.

Bennoun, M., Houari, M.S.A. and Tounsi, A. (2016), "A novel five variable refined plate theory for vibration analysis of functionally graded sandwich plates", *Mech. Adv. Mater. Struct.*, **23**(4), 423-431.

Bessaim, A., Houari, M.S.A. and Tounsi, A. (2013), "A new higher-order shear and normal deformation theory for the static and free vibration analysis of sandwich plates with functionally graded isotropic face sheets", *J. Sandw. Struct. Mater.*, **15**(6), 671-703.

Besseghier, A., Houari, M.S.A., Tounsi, A. and Hassan, S. (2017), "Free vibration analysis of embedded nanosize FG plates using a new nonlocal trigonometric shear deformation theory", *Smart Struct. Syst.*, **19**(6), 601-614.

Bouafia, K., Kaci, A., Houari M.S.A. and Tounsi, A. (2017), "A nonlocal quasi-3D theory for bending and free flexural vibration behaviors of functionally graded nanobeams", *Smart Struct. Syst.*, **19**(2), 115-126.

Bouderba, B., Houari, M.S.A. and Tounsi, A. (2013), "Thermomechanical bending response of FGM thick plates resting on Winkler-Pasternak elastic foundations", *Steel Compos. Struct.*, **14**(1), 85-104.

Bouderba, B., Houari, M.S.A., Tounsi, A. and Mahmoud, S.R. (2016b), "Thermal stability of functionally graded sandwich plates using a simple shear deformation theory", *Struct. Eng. Mech.*, **58**(3), 397-422.

Boukhari, A., Atmane, H.A., Tounsi, A., Adda Bedia, E.A. and Mahmoud, S.R. (2016), "An efficient shear deformation theory for wave propagation of functionally graded material plates", *Struct. Eng. Mech.*, **57**(5), 837-859.

Bounouara, F., Benrahou, K.H., Belkorissat, I. and Tounsi, A. (2016), "A nonlocal zeroth-order shear deformation theory for free vibration of functionally graded nanoscale plates resting on elastic foundation", *Steel Compos. Struct.*, **20**(2), 227-249.

Bourada, M., Kaci, A., Houari, M.S.A. and Tounsi, A. (2015), "A new simple shear and normal deformations theory for functionally graded beams", *Steel Compos. Struct.*, **18**(2), 409-423.

Bousahla, A.A., Benyoucef, S., Tounsi, A. and Mahmoud, S.R. (2016a), "On thermal stability of plates with functionally graded

coefficient of thermal expansion", *Struct. Eng. Mech.*, **60**(2), 313-335.
Bozyigit, B., Yesilce, Y. and Catal, S. (2017), "Differential transform method and Adomian decomposition method for free vibration analysis of fluid conveying Timoshenko pipeline", *Struct. Eng. Mech.*, **62**(1), 65-77.
Chikh, A., Tounsi, A., Hebali, H. and Mahmoud, S.R. (2017), "Thermal buckling analysis of cross-ply laminated plates using a simplified HSDT", *Smart Struct. Syst.*, **19**(3), 289-297.
Civalek, O. (2004), "Application of differential quadrature (DQ) and harmonic differential quadrature (HDQ) for buckling analysis of thin isotropic plates and elastic columns", *Eng. Struct.*, **26**(2), 171-186.
Dai, H., Wang, L., Qian, Q. and Ni, Q. (2014), "Vortex-induced vibrations of pipes conveying pulsating fluid", *Ocean Eng.*, **77**, 12-22.
Draiche, K., Tounsi, A. and Mahmoud, S.R. (2016), "A refined theory with stretching effect for the flexure analysis of laminated composite plates", *Geomech. Eng.*, **11**(5), 671-690.
El-Haina, F., Bakora, A., Bousahla, A.A. and Hassan, S. (2017), "A simple analytical approach for thermal buckling of thick functionally graded sandwich plates", *Struct. Eng. Mech.*, **63**(5), 585-595.
Esawi, A.M.K. and Farag, M.M. (2007), "Carbon nanotube reinforced composites: Potential and current challenges", *Mater. Des.*, **28**(9), 2394-2401.
Fiedler, B., Gojny, F.H. and Wichmann, M.H.G. (2006), "Fundamental aspects of nano-reinforced composites", *Compos. Sci. Technol.*, **66**(16), 3115-3125.
Garcı´a-Macı´as, E., Castro-Triguero, R. and Flores, E.I.S., (2016), "Static and free vibration analysis of functionally graded carbon nanotube reinforced skew plates", *Compos. Struct.*, **140**, 473-490.
Ghavanloo, E., Daneshmand, F. and Rafiei, M. (2010), "Vibration and instability analysis of carbon nanotubes conveying fluid and resting on a linear viscoelastic Winkler foundation", *Phys. E*, **42**(9), 2218-2224.
Hamidi, A., Houari, M.S.A., Mahmoud, S.R. and Tounsi, A. (2015), "A sinusoidal plate theory with 5-unknowns and stretching effect for thermomechanical bending of functionally graded sandwich plates", *Steel Compos. Struct.*, **18**(1), 235-253.
Heydarpour, Y., Aghdam, M.M. and Malekzadeh, P. (2014), "Free vibration analysis of rotating functionally graded carbon nanotube-reinforced composite truncated conical shells", *Compos. Struct.*, **117**, 187-200.
Hosseini, S.M. (2013), "Application of a hybrid mesh-free method based on generalized finite difference (GFD) method for natural frequency analysis of functionally graded nanocomposite cylinders reinforced by carbon nanotubes", *CMES-Comput. Model. Eng. Sci.*, **95**, 1-29.
Huang, Y.M., Liu, Y.S., Li, B.H., Li, Y.J. and Yue, Z.F. (2010), "Natural frequency analysis of fluid conveying pipeline with different boundary conditions", *Nucl. Eng. Des.*, **240**(3), 461-467.
Jam, J.E. and Kiani, Y. (2015), "Buckling of pressurized functionally graded carbon nanotube reinforced conical shells", *Compos. Struct.*, **125**, 586-595.
Jeong, W.B., Seo, Y.S., Jeong, S.H., Lee, S.H. and Yoo, W.S. (2007), "Stability analysis of a pipe conveying periodically pulsating fluid using finite element method", *Mech. Syst. Mach. Elem. Manufact.*, **49**(4), 1116-1122.
Khetir, H., Bouiadjra, M.B., Houari, M.S.A., Tounsi, A. and Mahmoud, S.R. (2017), "A new nonlocal trigonometric shear deformation theory for thermal buckling analysis of embedded nanosize FG plates", *Struct. Eng. Mech.*, **64**(4), 391-402.
Kiani, K. (2014), "Free vibration of conducting nanoplates exposed to unidirectional in-plane magnetic fields using nonlocal shear deformable plate theories", *Phys. E*, **57**, 179-192.
Lakis, A.A. and Sinno, M. (1992), "Free vibration of axisymmetric and beam-like cylindrical shells partially filled with liquid", *Int. J. Numer. Meth. Eng.*, **33**(2), 235-268.
Larbi Chaht, F., Kaci, A., Houari M.S.A. and Hassan, S. (2015), "Bending and buckling analyses of functionally graded material (FGM) size-dependent nanoscale beams including the thickness stretching effect", *Steel Compos. Struct.*, **18**(2), 425-442.
Lei, Z.X., Zhang, L.W. and Liew, K.M. (2015), "Vibration analysis of CNT-reinforced functionally graded rotating cylindrical panels using the element-free kp-Ritz method", *Compos. Part B: Eng.*, **77**, 291-303.
Liang, F. and Su, Y. (2013), "Stability analysis of a single-walled carbon nanotube conveying pulsating and viscous fluid with nonlocal effect", *Appl. Math. Model.*, **37**(10-11), 6821-6828.
Mahi, A., Bedia, E.A.A. and Tounsi, A. (2015), "A new hyperbolic shear deformation theory for bending and free vibration analysis of isotropic, functionally graded, sandwich and laminated composite plates", *Appl. Math. Model.*, **39**(9), 2489-2508.
Menasria, A., Bouhadra, A., Tounsi, A. and Hassan, S. (2017), "A new and simple HSDT for thermal stability analysis of FG sandwich plates", *Steel Compos. Struct.*, **25**(2), 157-175.
Meziane, M.A.A., Abdelaziz, H.H. and Tounsi, A.T. (2014), "An efficient and simple refined theory for buckling and free vibration of exponentially graded sandwich plates under various boundary conditions", *J. Sandw. Struct. Mater.*, **16**(3), 293-318.
Moradi-Dastjerdi, R. and Pourasghar, A. (2016), "Dynamic analysis of functionally graded nanocomposite cylinders reinforced by wavy carbon nanotube under an impact load", *J. Vibr. Cont.*, **22**(4), 1062-1075.
Mori, T. and Tanaka, K. (1973), "Average stress in matrix and average elastic energy of materials with misfitting inclusions", *Acta Metall. Mater.*, **21**(5), 571-574.
Mouffoki, A., Adda Bedia, E.A., Houari M.S.A. and Hassan, S. (2017), "Vibration analysis of nonlocal advanced nanobeams in hygro-thermal environment using a new two-unknown trigonometric shear deformation beam theory", *Smart Struct. Syst.*, **20**(3), 369-383.
Panda, L.N. and Kar, R.C. (2008), "Nonlinear dynamics of a pipe conveying pulsating fluid with combination, principal parametric and internal resonances", *J. Sound Vibr.*, **309**(3-5), 375-406.
Patel, S.N., Datta, P.K. and Sheikh, A.H. (2006), "Buckling and dynamic instability analysis of stiffened shell panels", *Thin-Wall. Struct.*, **44**(3), 321-333.
Raminnea, M., Biglari, H. and Vakili Tahami, F. (2016), "Nonlinear higher order Reddy theory for temperature-dependent vibration and instability of embedded functionally graded pipes conveying fluid-nanoparticle mixture", *Struct. Eng. Mech.*, **59**(1), 153-186.
Reddy, J.N. (2002), *Mechanics of Laminated Composite Plates and Shells: Theory and Analysis*, 2nd Edition, CRC Press.
Vakili Tahami, F., Biglari, H. and Raminnea, M. (2017), "Moving load induced dynamic response of functionally graded-carbon nanotubes-reinforced pipes conveying fluid subjected to thermal load", *Struct. Eng. Mech.*, **64**(4), 515-526.
Wang, L. and Ni, Q. (2009), "A reappraisal of the computational modelling of carbon nanotubes conveying viscous fluid", *Mech. Res. Commun.*, **36**(7), 833-837.
Wang, L. (2009), "A further study on the non-linear dynamics of simply supported pipes conveying pulsating fluid", *Int. J. Non-Lin. Mech.*, **44**(1), 115-121.
Yahia, S.A., Hassen, A.A., Houari, M.S.A. and Tounsi, A. (2015), "Wave propagation in functionally graded plates with porosities using various higher-order shear deformation plate theories", *Struct. Eng. Mech.*, **53**(6), 1143-1165.
Yu, D., Wen, J., Zhao, H. and Liu, Y. (2011), "Flexural vibration

band gap in a periodicfluidconveying pipe system based on the Timoshenko beam theory", *J. Vibr. Acoust.*, **133**(1), 1-3.

Zemri, A., Houari, M.S.A., Bousahla, A.A. and Tounsi, A. (2015), "A mechanical response of functionally graded nanoscale beam: An assessment of a refined nonlocal shear deformation theory beam theory", *Struct. Eng. Mech.*, **54**(4), 693-710.

Zhou, L., Chen, F. and Chen, Y. (2015), "Stability and bifurcation analysis of a pipe conveying pulsating fluid with combination parametric and internal resonances", *Math. Comput. Appl.*, **20**(3), 200-216

Zidi, M., Tounsi, A. and Bég, O.A. (2014), "Bending analysis of FGM plates under hygro-thermo-mechanical loading using a four variable refined plate theory", *Aerosp. Sci. Technol.*, **34**, 24-34.

CC